Journal of Marine Science and Application (2021) 20:426–445
https://doi.org/10.1007/s11804-021-00219-w

RESEARCH ARTICLE

A Comprehensive Analysis of the Stability and Powering Performances of a Hard Sail–Assisted Bulk Carrier

Md Daluar Hussain[1] · Osman Md Amin[1]

Received: 12 June 2020 / Accepted: 9 June 2021 / Published online: 10 August 2021

Abstract

The wind-assisted propulsion system is becoming one of the most popular and efficient ways to reduce both fuel consumption and carbon dioxide emission from the ships. In this study, several analyses have been carried out on a model of bulk carrier fitted with five rigid sails with a 180° rotating mechanism for maximum usage of wind power and a telescopic reefing mechanism for folding it during berthing. The stability of the ship has been verified through the calculations of initial stability, static stability, and dynamic stability through the fulfillment of the weather criterion using MAXSURF software. The structural analysis of the sail was carried out in ANSYS static structural module. Several flow simulations were carried out in ANSYS fluent module to predict the thrusts produced by the sails at different apparent wind angles, which would in turn reduce the thrust required from the propeller. In this way, the brake horse powers required for different sail arrangements were analyzed to find out a guideline for this wind propulsion system to generate better powering performances. To consider drift and yaw effect on propulsion system, an MMG mathematical model–based simulation was carried out for different drift angles of motion of the ship considering hard sail–based wind loads. Through these analyses, it has been found out that the hard sail–based wind-assisted propulsion system in some cases have produced a reduction of more than 30% brake power in straight ahead motion and around 20% reduction in case of drifting ships compared to the model having no sails.

Keywords Wind-assisted propulsion system · Fuel consumption · Brake power · Carbon dioxide emission · Wing sail · Bulk carrier · Sail ship stability · CFD simulations

1 Introduction

Transporting about 90% of the tonnage of all traded goods, the shipping industry has been the backbone of the world trade and lifeline for modern cities since the dawn of civilization. The global shipping tonnage increased from 2.6 to 9.2 billion tons between 1970 and 2012 (Mofor et al. 2015). The world seaborne trade gathered momentum in 2017 with volumes expanding up to 4%, the fastest growth in 5 years, which is estimated at 10.7 billion tons. Further, global trade by shipping is projected to expand at a compound annual growth rate of 3.8% between 2018 and 2023 (IMO 2014). However, the concerns associated with the world shipping industry are the environmental issues as well as the increase of the high price of fuel oil.

The unsteady however usually rising prices of marine fuels account for a large proportion of the running costs of a ship. In March 2014, the price of heavy fuel oil was 600 USD/MT whereas in February 2015 it drops to 325 USD/MT, where in recent times it is increasing again. In the same period, the

Article Highlights
- Sail-based wind-assisted propulsion system of ship to reduce emissions and fuel consumption has been investigated thoroughly in this article.
- More than 30% reduction in brake power and fuel consumption for this system is predicted.
- Stability of a sail-assisted ship is assessed considering weather criteria.
- Forward thrust gain by the rigid sails is estimated by CFD simulation considering sail–sail interaction.
- The effects of drift and yaw on the sail performance are investigated using MMG model for ship maneuvering along with Fujiwara's wind model.

✉ Md Daluar Hussain
dhsumon014mist@gmail.com

[1] Department of Naval Architecture and Marine Engineering, Military Institute of Science and Technology (MIST), Dhaka 1216, Bangladesh

price of low-sulfur fuel has dropped from 950 to 600 USD/MT, which provides an expensive alternative to the power sources for the shipping community (Lloyd's Register 2015). The other concern related to environmental issue is more alarming. A ship may pollute the environment in various ways such as air pollution, water pollution, and ground pollution on voyages as well as pollution on ship recycling. In spite of being the most efficient modes of global transportation compared to other modes like air and roadways, shipping contributes to the emission of CO_2, NO_x, and SO_x at about 2%–3%, 10%–15%, and 4%–9% per year, respectively. If it continues, the amount of global CO_2 emission can be increased up to 250% within the year 2050 (IMO 2014).

In July 2011, IMO MEPC 62 adopted a set of regulations to be included into MARPOL ANNEX VI to make Energy Efficiency Design Index (EEDI) mandatory for new ships to measure the energy efficiency of the ships taking into account of the ship's emissions, capacity, and speed. According to the requirement of EEDI, the newest ship should be 20% more efficient by 2020 and 30% more efficient from 2025 in terms of reduction of CO_2 emission along with overall air pollution (IMO 2014). The CO_2 output has a proportional relationship with fuel consumption; hence, the reduction of fuel consumption reduces the CO_2 footprint. Thus, to maintain EEDI, the fuel-efficient ships are suggested to reduce CO_2 emission and the high price of the fuel oil. Slow streaming has now become the principal method to reduce fuel consumption and emission by global shipping. However, the reduction of the speed and corresponding fuel consumption do not relate to an equivalent percentage increase in efficiency.

The reduction of fuel consumption can be achieved by introducing various methods such as liquefied natural gas (LNG)–fueled propulsion, renewable energy utilization (using wind and solar power), improved design (optimized hull form design, highly efficient propeller design, bulbous bow optimization), various energy-saving devices (waste heat recovery system, NO_x and SO_x reduction devices), use of advanced anti-fouling paint, and optimum weather routing (Mofor et al. 2015). A combined approach of these aspects will surely advance the industry toward zero emission and greener shipping. Among the various fuel-efficient technologies available to face these challenges, wind-based technologies are the ones having the potential for double-digit fuel savings as well as reduction of the GHG emissions.

2 Literature Review: Wind-Assisted Ship

Due to the limitation in utilization of wind velocity for the fully dependent wind propulsion systems along with the availability and cheap price of fuel oil combined with less concern about environment and improvement of the marine engines, the merchant sailing ship became obsolete at the beginning of twentieth century. However, the crisis of fuel and sudden rise of fuel price in 1970s led the shipping industry to grow interest toward the wind-assisted propulsion system to reduce fuel consumption (Lloyd's Register 2015). In 1980, the Royal Institute of Naval Architecture (RINA) arranged a conference in UK titled "The Symposium on Wind Propulsion in Commercial vessels" and another conference in 1985 titled "The symposium on Wind Propulsion Technology" was arranged by the same institution to introduce these technologies in its modern form. In 1980, the US government commissioned a study for the economic feasibility of various possible wind-assisted propulsion systems and wing sail concept was concluded as the most beneficial one (Bockmann 2015). In the year 1970, "The Shin Aitoku Maru," a 70-m oil tanker, was constructed and run by JAMDA Japan that is considered the pioneer of the modern sail-assisted ship, in which two rigid wing sails were used and the amount of fuel savings was found to be within 10%–15% of total fuel consumption (Ouchi et al. 2011). The inspiration of the success of the Shin Aitoku Maru led to build 17 vessels up to 1994 using similar technologies (Ouchi et al. 2011). A cargo ship was built in 1986 using rigid sail, which was able to save the fuel consumption rate from 15% to 30% (Lloyd's Register 2015).

Methods that use the wind to provide energy to drive ships include a variety of modern techniques. Typically, these adopt Flettner rotors, kites or spinnakers, soft sails, wing sails, and wind turbines. Numerous concepts on rigid sail have additionally been applied to a spread of smaller vessels; however, these have not gained widespread acceptance thus far on either large ship because of varied engineering and operational challenges. Wind-assisted propulsion can significantly lower fuel consumption and emissions, but the main challenges of the economics highly depend on wind conditions, ship types, and shipping routes (Tillig and Ringsberg 2020). The low-speed ocean-going bulk carriers and oil tankers can particularly benefit from wind-assisted propulsion as low-speed operation increases the spectrum of wind directions where soft sails and wing sails can generate useful thrust (Viola et al. 2015). Various wing sail ship technology concepts of both soft sails and rigid sails have also been developed in recent years. OCIUS Technology claims that without modifying a modern tanker or bulker's primary propulsion system, a retrofitting opening wing sails to can save 20%–25% on cross-equator shipping routes and 30%–40% on transatlantic shipping routes (Nuttall and Newell 2015). Seagate, an Italian company, has patented folding delta wing sails that can be retrofitted to existing ships such as Ro-Ros, containerships, and car carriers, resulting in fuel savings of up to 19% (Nuttall and Newell 2015). WindShip, another WAPS technology provider, claims that their recent designs for a motor sailing system with modern fixed wings would reduce fuel costs by 30% (Nuttall and Newell 2015). Full-scale tests showed that kites used together with conventional engines could enable an

annual saving of up to 35% although it has difficulties in launching and landing as well as the requirement of a wide air space (Viola et al. 2015). Enercon, which deals in wind energy generation and technology, launched a Flettner-rotor powered cargo ship named the E-Ship-1 in 2008, and it is reported that this device helped to reduce fuel consumption by 25% compared to conventional systems (Schmidt 2013). Norsepower, another company that deals with the wind propulsion system of ships, began prototyping a practical Flettner rotor system, and the device has been installed on a number of ocean-going vessels in which 5%–20% reduction of fuel consumption is achieved (Norsepower 2019). A recent study on a tanker and a RoRo with Flettner rotor has showed that a fuel savings of 30% can be achieved for the tankers and 14% can be achieved for the RoRo considering the four-degrees-of-freedom (4-DOF) performance of ships in realistic weather conditions (Tillig and Ringsberg 2020). The latest researches ensure that fixed sails with the integration of modern techniques are probably the most efficient and cost-effective way to use wind energy as compared to other options where the drawback of fixed sails is the possible obstruction in sight from the bridge (Lloyd's Register 2015). In a nutshell, a list of various state-of-the-art wind-assisted fuel-saving technologies with their current status is presented in Table 1.

Table 1 Current projects/technologies on wind-assisted ship propulsion (Lloyd's Register 2015; Mofor et al. 2015; Carlsson and Roggers 2017; Atkinson 2012; Mohit 2017; IWSA 2016)

Name of the technology	Expected fuel savings (%)	Projects/concepts/ technologies provider	Current status
Rigid wing sails	10–40	Eco Marine Power	Concept, design, CFD simulation
		Wind Ship Technology	
		Wind Ship Powered by Nature, UK	
		Ocean Foil Wing Sail Technology	
		Propel-wind, France	
		MOL Wind Challenger (Wind Challenger Project)	Detail design and software development for control mechanism
		NAYAM wings	Model test completed successfully, intending to start construction
Square rig sail systems (Dyna-R-ig)	Up to 50	B9 Sail Cargo Ship Dykstra Naval Architects	Concept for new build ship
Towing kites	10–30	Maltese Falcon	In operation since 2006
		SkySails Marine	One ship in operation
		Beyond the sea	Concept, Design, CFD simulation
Flettner rotors	20–30	M/V Estraden ro-ro by Norsepower Oy Ltd E-Ship 1	In operation
	35–50	Magnuss Voss Wind Hybrid Coaster Anemoi Flettner rotors	Construction

A common approach in high-performance sail ships is to solve the coupled equations of motion with the Velocity Prediction Program (VPP) which are essential design tools to compare different candidate design solutions (Viola et al. 2015). Fujiwara et al. (2003a) studied the aerodynamic characteristics of multiple wing sails and carried out a wind tunnel experiment to reveal the sail–sail and sail–hull interaction effects of a hybrid sail. In case of a sail-assisted ship, a heeling will occur owing to the wind loading of the sail installed on deck; therefore, roll motion must be adressed in additon to surge, sway, and yaw (Fujiwara et al. 2005). VPPs have been implemented on ships with wing sail by Ouchi et al. in Ouchi et al. 2011 and an Energy Prediction Program (EPP) was developed to evaluate ship performance with wing sail. A performance prediction program is presented by Bordogna et al. (2014), considering the aerodynamic interaction effects of wind propulsion systems as well as the hydrodynamic phenomena heel, leeway, side force, and yaw balance. A 4-DOF ship performance prediction model has been used by Lu and Ringsberg (2019) to compare three wind-assisted ship propulsion technologies: the Flettner rotor, a wingsail, and the DynaRig concept. A 4-DOF ship performance prediction model called "ShipCLEAN" has been developed by Tillig and Ringsberg (2020), which includes aero- and hydrodynamic interaction and a method for rpm control of Flettner rotors on a ship to maximize fuel savings. The modern wind-assisted propulsion concepts combine proven principles with advances in automation, control systems, weather routing, and materials, while advances in computational fluid dynamics (CFD) and wind tunnel testing enable their performance to be predicted and optimized more reliably (Lloyd's Register 2015; Van der Kolk et al. 2019).

In the present paper, a CFD-based study has been carried out to predict the amount of forward thrust generated by sails. In CFD simulations, the effects from drift and yaw on the sail performance and propulsive coefficients are neglected. Furthermore, ship motion equations have been solved for ship with sail for a constant ship speed to consider the interaction effects of drift and yaw on the sail performance. In addition to calculation of the forward thrust by rigid sails, reduction in brake power, and specific fuel consumption (SFC), the stability of the ship with wing sail considering wind heeling

moment and structural analysis of the sail using FEM have been investigated.

3 Physics of Sail-Assisted Ship

A typical schematic diagram has been shown in Figure 1 through the depiction of the body fixed coordinate system along with the direction of wind and forces acting on the sail and hull. The sail in the wind acts as an airfoil and the hull in the water acts as a hydrofoil, so there are two sets of forces acting on a sail ship: aerodynamic and hydrodynamic. The lift and drag force generated by the sails are resolved into a total aerodynamic force which gives the thrust froce to drive the ship forward. The hydrodynamic force has two parts; one is the forward thrust which is often known as driving force too and another one is the sideway force. These forces are calculated by the formulae given (1) to (6).

The apparent wind speed and apparent wind angle are calculated by using the following formulas (Hu et al. 2015a, 2015b):

$$V_a = \sqrt{V_s{}^2 + V_t{}^2 + 2V_sV_t\cos\,(\mathrm{TWA})} \tag{1}$$

$$\tan(\mathrm{AWA}) = \frac{V_t \sin\,(\mathrm{TWA})}{V_s + V_t \cos\,(\mathrm{TWA})} \tag{2}$$

In Figure 1, Φ denotes apparent wind angle (AWA), θ sail rotating angle, α sail attack angle, V_a apparent wind speed (AWS), V_s ship speed, and V_t true wind speed (TWS).

The forward thrust generated by wing sail is calculated by using the following formula (Hu et al. 2015a, 2015b):

$$T = C_T \times 0.5 \times \rho \times A_s \times V_a^2 \tag{3}$$

The sideway force generated by wing sail is calculated by using the following formula (Hu et al. 2015a, 2015b):

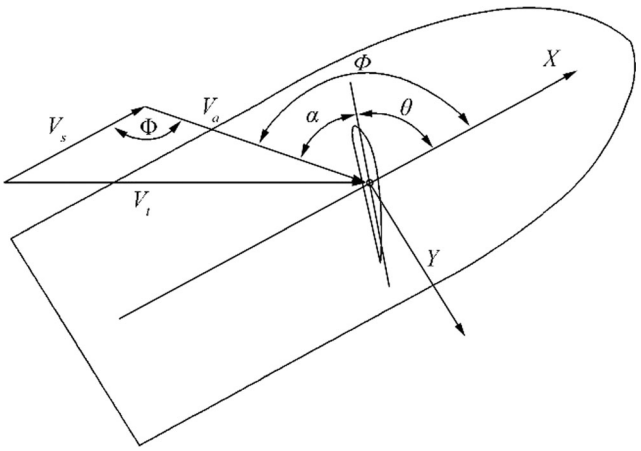

Figure 1 Coordinate system for sail-assisted ship (Hu et al. 2015a, 2015b)

$$F_H = C_H \times 0.5 \times \rho \times V_a^2 \times A_s \tag{4}$$

The thrust coefficient is calculated by using the following formula (Hu et al. 2015a, 2015b):

$$C_T = C_L \sin\Phi - C_D \cos\Phi \tag{5}$$

The sideway force coefficient is calculated by using the following formula (Hu et al. 2015a, 2015b):

$$C_H = C_L \cos\Phi + C_D \sin\Phi \tag{6}$$

where C_T is thrust coefficient, C_H is sideway force coefficient, ρ_a is density of air, A_s is area of the sail (m^2), Φ is angle between wind and ship (apparent wind angle) as defined in Figure 1, C_L is lift coefficient, and C_D is drag coefficient.

4 Work Methodology

The methodology which was followed to carry out the study is given in Figure 2.

5 Selection of Ship Hull and Sail Design

5.1 Ship Hull Selection

For this analysis, the hull of Japan Bulk Carrier (JBC) (Figure 3) was chosen. The JBC is a Cape-size bulk carrier whose hull, propeller, and rudder were designed jointly by the National Maritime Research Institute (NMRI), Yokohama National University, and Ship Building Research Centre of

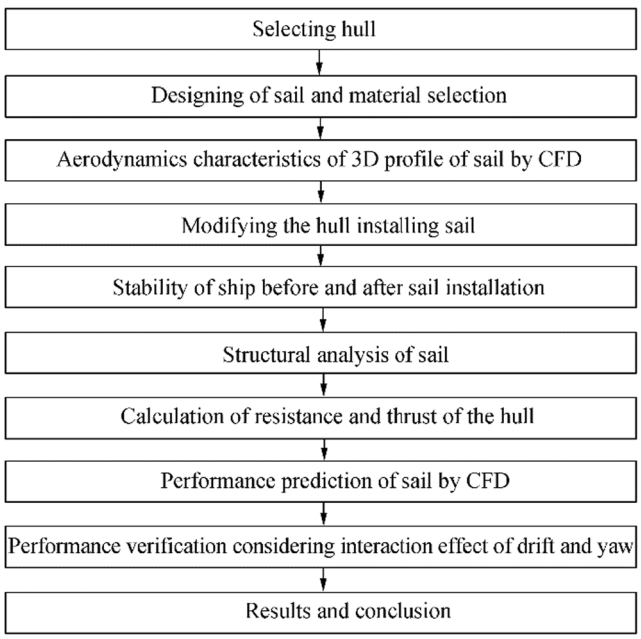

Figure 2 Work Methodology

Japan (SRC). Towing tank experiments were planned at NMRI, SRC, and Osaka University, which included resistance tests, self-propulsion tests, and PIV measurements of stern flow fields. The resistance test data for model scale ship has been used in this analysis for the calculation of reduction in required thrust and brake power. The principal particulars of the ship have been shown in Tables 2, 3.

The resistance of JBC was predicted through various cases in both experimental and CFD simulation. The frictional resistance coefficient was calculated by using ITTC 1957 formula and the wave making resistance coefficient was used from experimental data as shown in Figure 4 at a speed of 1.179 m/s. The summary of the calculated values of total resistance and power for the model ship has been given in Table 4.

5.2 Sail Design Consideration

The wing sail can be classified into many ways on the basis of shape and type of material used to make it. The shape and material optimization are one of the major challenges for modern wing sail ship. In designing the rigid wing sail, the following aspects used are to be taken into consideration:

1. Higher thrust and performance efficiency, i.e., good aerodynamic performance;
2. Capability of utilizing the wind at various wind conditions;
3. Ability to withstand at various weather conditions;
4. Dimension and mechanism of folding the mast, as the upper part of sail faces the stronger velocity than the lower part and the mast support the weight of the sail;
5. Simple structure and less weight, simple control mechanism;
6. Optimum larger sail area preferred considering space, stability of ship, visibility, and maneuvering;
7. Cost-effectiveness.

5.3 Sail Profile Selection

In case of huge hard wing sail, the performance mostly depends on the sail cross-sectional profile. The degree of curvature (camber) of the profile when aligned with the apparent

Table 3 Propeller particulars (NMRI 2015)

Particulars	Full scale	Model scale
Propeller diameter (m)	8.12	0.203
Expanded area ratio, A_E	0.50	0.50
Number of blades	5	5
Maximum blade area ratio	0.2262	0.2262
Pitch (m)	6.09	0.15225
P/D	0.75	0.75

Table 2 Main particulars of ship (NMRI 2015)

Particulars		Full scale	Model scale
Length between perpendiculars, L_{PP} (m)		280	7
Length of waterline, L_{WL} (m)		285	7.125
Breadth, B (m)		45	1.125
Depth, D (m)		25	0.625
Draft, d (m)		16.5	0.4125
Displacement, Δ (t)		182 829.1	2.787
Block coefficient, C_B		0.858	0.858
Midship coefficient, C_m		0.9981	0.9981
Waterplane area coefficient, C_m		0.925	0.925
Prismatic coefficient, C_p		0.86	0.86
Speed, v_m (kn)		14.5	2.294
Wetted surface area w/o ESD (m^2)		19,556.1	12.222
LCB (% L_{PP}), fwd+		2.5475	0.064
Metacentric height, GM (m)		5.3	0.1325
Moment of inertia	I_{XX} (kg·m^2)	5.924×10^{10}	564
	I_{YY} (kg·m^2)	8.959×10^{11}	8535
	I_{ZZ} (kg·m^2)	8.959×10^{11}	8535
Added mass, m_x (5% of Δ) (t)		9141.455	0.13935
Added mass, m_y (t)		138 950	2.11812
Added moment of inertia, (kg·m^2)		42.7984	0.627

(a) Body plan view of the JBC (b) Profile view of the JBC (NMRI, 2015)

Figure 3 Selected ship hull form. **a** Body plan view of the JBC. **b** Profile view of the JBC (NMRI 2015)

wind (the angle of incidence) produces maximum drive. For this analysis, the NACA 4412 as shown in Figure 5 section is chosen for the sail profile by analyzing their proven performance as wing sail. NACA 4412 with a chord of 20 m has

1. Maximum camber: 0.8 m (4% × 20 m);
2. Location of maximum camber: 8.0 m aft of leading edge (0.4 × 20 m);
3. Maximum thickness: 2.4 m (12% × 20 m).

In Table 5, the particulars of the sail for both case of full scale and model scale have been shown. The sail particulars and sail-to-sail distance were determined on the basis of the wing sails used in UT wind challenger (Ouchi et al. 2011). A segmented 3D drawing of the sail has been shown in Figure 6a. The wing sails have vertically telescopic reefing mechanism and also self-rotating mechanism to meet the required wind direction. The vertical telescopic sail has five segments so it can be contracted and expanded, when necessary, especially when the ship is in port or in berthing or in rough weather condition.

5.4 Material Selection for the Sails

Material must be of such type that it will have good mechanical properties, higher strength, corrosion resistance, and obviously cost-effectiveness. The rigid hard sail must be capable to withstand high wind velocity such as 25–30 m/s at sea. Different material can be chosen for different parts of the sail. By reviewing recent research works on rigid wing sail materials like carbon fiber reinforced polymer composites (CFRP), aluminum steel and stainless steel are chosen to be the better options for the main body of sail (Ouchi et al. 2011). The CFRP is very light in weight and has excellent strength but is quite expensive compared to other options for materials. For telescopic mast low alloy steel, glass reinforced plastics (GRP) and stainless steel are mentionable materials (Hu et al. 2015a, 2015b). Low alloy steel is preferred for the mast by considering their proven performance. In this analysis, the CFRP for the segmented sail exposed body and the ordinary alloy steel for the mast were chosen as preliminary choice for their proven performance of these applications.

Table 4 Calculated resistance and power values

Parameters	Value
Model ship speed, v_m (m/s)	1.179
Frictional resistance coefficient, C_F (ITTC 1957)	0.00316
Wave making resistance, C_W	0.00015
Form factor (1+k)	1.314
Total resistance coefficient, C_T	0.00331
Total resistance, R_T (N)	28.11
Effective power, P_E (W)	33.14
Brake power, P_B (W)	47.34

5.5 Aerodynamics Characteristics of 3D Sail

The aerodynamic characteristics of the sail can be observed from the lift and drag force coefficient of the sail. The lift and drag force coefficient of a single sail are determined by CFD simulation in ANSYS Fluent to observe their characteristics. In this case, a single sail was taken without considering navigation speed of vessel to obtain lift and drag coefficient. The sail was scaled down to 1:12.

The lift and drag coefficients were obtained for wind velocity 6 m/s for the sail angle of attack of 0, 15, 30, 45, 60, 75, and 90°. Here, 6 m/s wind velocity for sail is equivalent to 21 m/s for full-scale sail. While simulating by CFD using ANSYS fluent of a 3D sail, the sail was taken as a simplified sail that has no segment as shown in Figure 7. As the 3D sail was scaled down to 1:12 for the CFD simulation, the height of the sail became 4 m and the chord became 1.67 m.

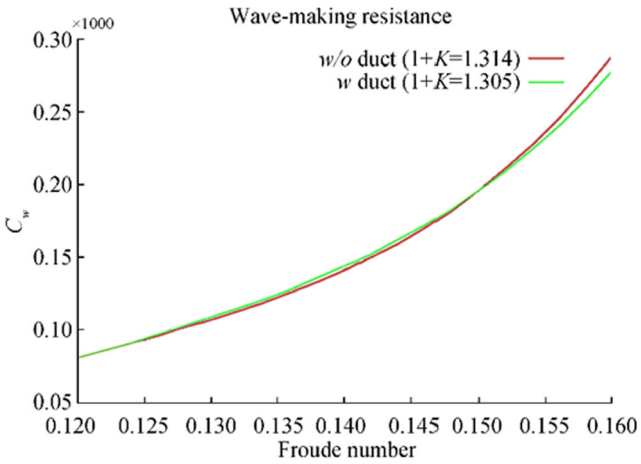

Figure 4 Wave making resistance coefficient (Nobuyuki 2015)

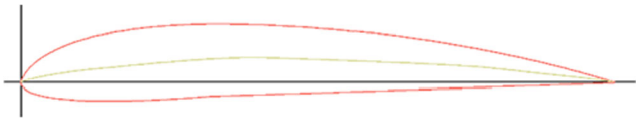

Figure 5 NACA 4412 profile (http://airfoiltools.com/airfoil/details?airfoil=naca4412-il)

The pattern of graph (Figure 8) shows that the value of drag coefficient increases while increasing the wind attack angle on sail, but in case of lift coefficient, the value increases up to sail attack angle 18° and then gradually decreases. The lift coefficient value at sail attack angle zero is about 0.08. C_L reaches its extreme, namely the inflection at a curve turning point, when the sail attack angle is around 18°. The maximum thrust-producing angle is about 18° for a single isolated sail, which is often considered the maximum lift point. Moreover, the effective optimum angle of attack depends on the full system including added resistance from waves and drifting. In case of determining the thrust generated by the sails, the values obtained for single sail cannot be used because there will be interaction of wind flow among the sails which will give different lift and drag force at different sails. However, it was calculated to observe the initial characteristics of the sail section. Moreover, these lift and drag values were used to calculate heeling force and moment to evaluate preliminary stability analysis at high wind speed of ship with wing sails as described in the next section.

6 Stability of Sail-Assisted Ship

One of the most important requirements of modern wind-assisted ship is that the stability of a ship must not be affected significantly by the sails at high wind speeds. A ship is always acted upon by several external forces like wind and wave along with internal forces which sometimes may adversely affect the ship's intact stability. Wind works against the stability. The intact stability characteristic of a sail-assisted ship is slightly different from a ship without sail due to the action of forces and moments acting on large area of sail. The steady and gust components of wind contribute to increase the rolling motion (Clearly et al. 1996). The sail forces and moments due to relative wind flow on it may increase the rolling angle of ship. A lack of adequate intact stability may cause the capsizing of the large sailing ships. So, the stability analysis has done to check stability condition of the designed sail-assisted ship with sail in both full load and light weight condition.

Table 5 Main particulars of sail

Particulars	Full scale	Model scale
Sail span (m)	48	1.2
Sail chord (m)	20	0.5
Aspect ratio	2.4	2.4
Maximum thickness (m)	2.4	0.06
Maximum camber (m)	0.8	0.000625
Mast diameter (m)	0.5	0.0125
Projected Surface area (m^2)	860	0.6

6.1 Sail Ship Stability Criteria

There are several criteria and methods to evaluate the stability of sail-assisted ship as proposed by Lloyd's/Wolfson, Germanischer Lloyd's (GL), Bureau Veritas (BV), United Sates Coast Guard (USCG), and Ateliers et Chantiers du Havre (ACH). In a very recent paper, the stability criteria of sail-assisted ship as recommended by Hu et al. (2015a, 2015b) are used in this analysis. The recommended stability criteria on sail assisted ship are as follows:

1. Weather criteria, $K \geq 1$;
2. Metacentric height, GM >0.3 m.

The weather criteria K for the sail-assisted ship are suggested as the ratio of maximum heeling moment (M_q) to wind heeling moment (M_f), i.e., $K = M_q/M_f$.

6.2 Stability Calculation

Maximum heeling moment is defined as the moment up to which a ship can withstand at severe condition of wind. The maximum heeling moment (M_q) is formulated as follows (IMO 2008):

$$M_q = h_2 \times \Delta \tag{7}$$

where Δ is vessel displacement in tons and h_2 is gust wind heeling arm as shown in Figure 9.

The wind heeling moment (M_f) consists of two parts where one is the moment acting on ship structure due to wind (M_{fb}) and another one is moment acting on sail due to wind (M_{fs}) which can be formulated as (Hu et al. 2015a, 2015b)

$$M_f = M_{fb} + M_{fs} \tag{8}$$

where the moments are expressed in kilogram-meter.

To calculate the wind heeling moment on ship and superstructure, the empirical method to calculate wind forces and moment acting on ship proposed by Fujiwara et al. (1998) is used. According to that method, the heeling moment due to wind is calculated by using the following formula:

$$M_{fb}(K) = C_k \times q \times A_L \times H_L \tag{9}$$

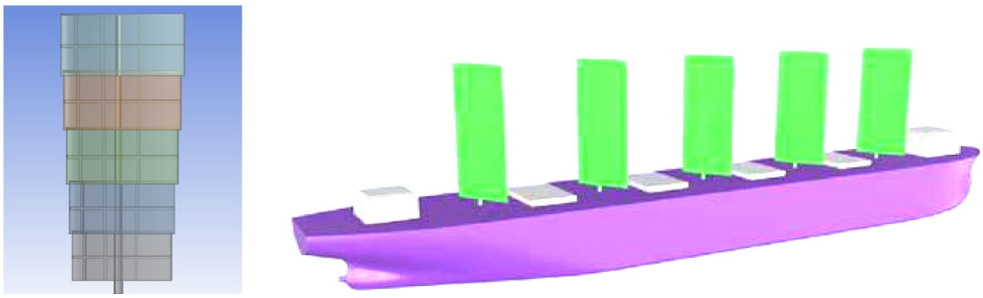

(a) Front view of sail

(b) Simplified 3D model of JBC with sail

Figure 6 Sail design and arrangment in ship. **a** Front view of sail. **b** Simplified 3D model of JBC with sail

C_k is calculated by the empirical formula proposed by Fujiwara et al. (1998) where the formula has been generated using experimental data of two ships for different types of parameters. The heeling moment due to sail is determined by using the expression (Hu et al. 2015a, 2015b)

$$M_{fs} = Fs \times Z_1 = 0.5 \times \rho \times V_b{}^2 \left(C_L \sin \Phi + C_D \cos \Phi\right) \times Z_1 \quad (10)$$

The lift coefficients, C_L, and drag coefficients, C_D, of the sail for different angles of attack and velocities are calculated by CFD simulation in ANSYS fluent.

The stability was calculated for various wind angles ranging from 0 to 90° and for different wind speeds ranging from 6 to 16 m/s (Figure 10). The focus was on the cases for which the maximum heeling moment can occur. Hence, the maximum values obtained are listed here as a consequence of the results. In Table 6, the summary of calculated heeling moments has been shown, where α indicates sail attack angle and Φ wind angle between ship centerline and sail. It is seen from Table 6 that for the case, where both α and Φ are 90° with wind speed 16 and 14 m/s, the value of K, i.e., M_q/M_f, is less than 1. In another case where A is 90° and Φ is 70° for wind speed 16 m/s, the ratio of moments is less than 1. These are cases when the designed sail-assisted ship becomes unstable.

6.3 Stability Analysis in MAXSURF

The intact stability curves for both before and after sail installation were obtained using MAXSURF Stability Enterprise software. The IMO criteria MSC 267 (85) code on intact stability was used to do the large angle stability analysis in lightship condition (with sail) and at full load condition (with and without sail), as can be seen in Figure 11, respectively. Table 7 shows various intact stability criteria results obtained using the IMO criteria of MSC 267 (85) code in MAXSURF software for various loading conditions of the ship.

It is seen that from the table, the value of initial metacentric height decreased after the sail installation. Before the sail installation at full load condition, it was about 5.702 m and after sail installation it becomes about 5.185 m. The value of maximum GZ before sail installation is 3.309 m and after sail installation it is about 3.155 m. One of the important things is that the value of maximum GZ occurs at the same angle which is about 40.9° for both cases. The comparison of area under the GZ curve within 0–0°, 0–40°, and 30°–40° has also been shown in Table 7.

7 Structural Analysis of the Sail

It is expected that the optimum wind speed for the operation of sail in full scale will be 11–12 m/s. Although we have considered the maximum wind speed to be 16 m/s for stability analysis, a maximum wind pressure for 20 m/s was considered for the structural analysis. It has been estimated that the wing sails are exposed to the wind pressure about 228 N/m^2 in case of 15 m/s wind speed and 405 N/m^2 in case of 20 m/s wind speed. The drag coefficient has been taken for 90° sail attack angle (Figure 8) and the force coefficient has been calculated using

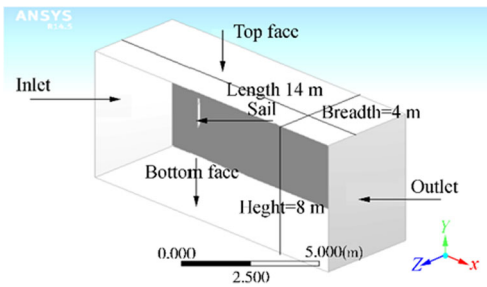

Figure 7 Numerical domain for single sail

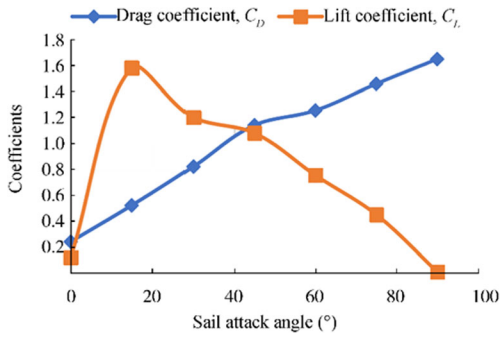

Figure 8 Lift and drag coefficients for single sail

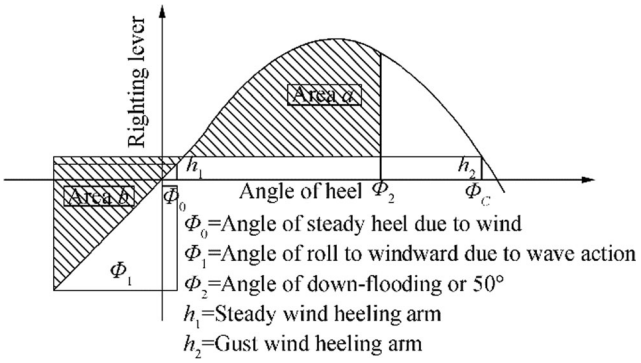

Figure 9 Righting lever curve with wind heeling arm (IMO IS Code 2008)

Eq. (6). The wind force per unit area is obtained from Eq. (3) using the force coefficient. The total exposed area of the sail approximately 860 m^2 and the total weight of sail with mast is approximately 80 t. The properties of the selected material have been given in Table 8.

The 3D design of the sail was modeled in SolidWorks and imported into ANSYS Workbench software. Static structure module was used to carry out the structural analysis. The unstructured tetrahedron dominant mesh was generated using ANSYS Static Structure mesh tool. Program controlled triangular meshing method was used as patch conforming option. Mesh based on defeaturing was enabled and was set as default. Total number of nodes and elements were taken 2 960 135 and 1 579 835 respectively. The sail with mast is generally considered like a cantilever beam where the end of the mast acts as a fixed end. In actual case, this end is fixed with the main deck of ship. Although the distribution of wind pressure will vary along with span of the sails from bottom to top, it is taken uniformly distributed instead of varying loads as the variation is not a large amount. The uniformly distributed pressure has been applied to the positive *Y*-direction to the normal direction of the face of sail as shown in Figure 12a.

The sail has been statically analyzed to find the total deformation and the equivalent stress (Von-Mises stress). From the analysis, maximum deflection/deformation and equivalent stress were obtained for the pressure at 15 and 20 m/s wind speed. The boundary condition and loads were applied according to Figure 12a. The number step was taken 1 as the required values were obtained only for loading condition. In solution menu, solver output was set as iterative and the large deflection was enabled. It is notable that the stress value is maximum at the mast of the sail in both cases, whereas at the main body of the sail, the stress is lower. The obtained maximum and minimum values have been given in Table 9.

Table 6 Heeling moments and weather criteria

AWA (°)	AWS (m/s)	M_{fb} (kg·m)	M_{fs}(kg·m)	M_f (kg·m)	M_q/M_f
	16	3 146 068	3 684 096	6 830 164	0.702911
$\Phi = 90$	14	2 408 708	2 820 636	5 229 344	0.918088
$A = 90$	12	1 734 270	2 047 032	3 781 302	1.269669
	10	1 204 354	1 421 550	2 625 904	1.828323
$\Phi = 90$	16	2 623 134	3 537 328	6 160 462	0.779325
$A = 70$	14	2 008 337	2 708 258	4 716 594	1.017895
	12	1 475 513	1 989 747	3 465 260	1.385466
	10	1 024 662	1 381 769	2 406 431	1.995071

8 Thrust Calculation and Performance Prediction of Sail by CFD

The lift and drag coefficient are obtained by CFD simulation of five sails together in model scale in ANSYS Fluent software module. Considering the interactions among sails, the five sails were arranged for different combinations of orientations considering the line joining the CG of sail as centerline of the ship. Since the experimental data on the power requirement and resistance of the JBC ship hull model can be found out from the literature, the hull was not considered in CFD simulation. The CFD simulation of sails was carried out for the sail after scaling in the same scale as the ship (1:40) and the detail dimension of model sail and model ship are given earlier in Table 5.

8.1 Governing Equations

The well-known Navier–Stokes's equation of motion for a two-dimensional, compressible, and viscous fluid may be written in the following form (Menter 1994):

Continuity Equation:

$$\frac{\partial \rho}{\partial t} + \frac{\partial (\rho u_i)}{\partial x_i} = 0 \tag{11a}$$

Momentum Equation:

$$\frac{\partial (\rho u_i)}{\partial t} + \frac{\partial \left(\rho u_i u_j\right)}{\partial x_j} = -\frac{\partial p}{\partial x_i} + \frac{\partial \left(\tau_{ij}\right)}{\partial x_j} + \rho f_i \tag{11b}$$

In the above momentum equations, for Newtonian fluid the stress terms are proposed by Stokes as

$$\tau_{ij} = \mu\left(\frac{\partial u_i}{\partial x_j} + \frac{\partial u_j}{\partial x_i}\right) - \frac{2}{3}\delta_{ij}\frac{\partial u_k}{\partial x_k} \tag{11c}$$

where ρ is the fluid density; t is time; x is the position vector; u is the fluid velocity; i, j, and k are the coordinate directions; p is the pressure; f is the body force; τ is Newtonian stress; μ is the dynamic viscosity of the fluid due to laminar diffusion; and δ is the Kronecker delta function.

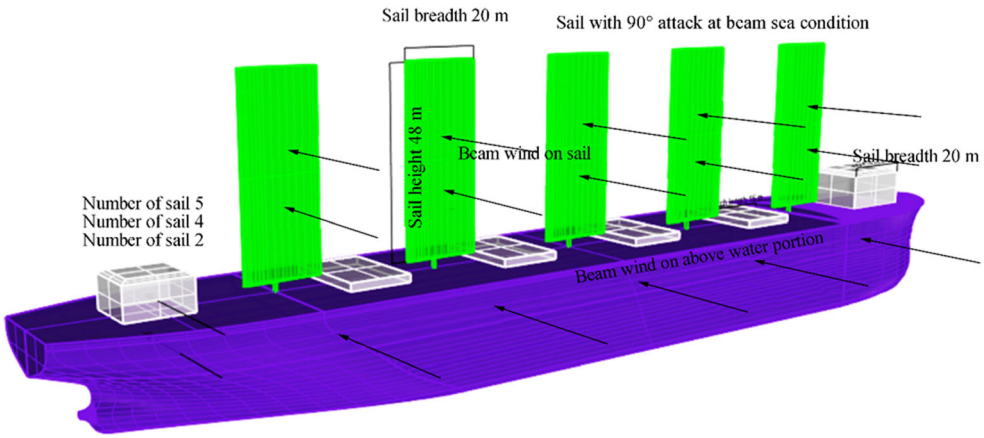

Figure 10 Ship with sail at beam wind

8.2 Algorithm and Difference Scheme

To determine the thrust generated by the sail system consisting of five individual sails, steady RANS (Reynolds Averaged Navier–Stokes) solver is being adopted through the use of ANSYS Fluent software by simulating the flow field around the sails. On the basis of finite volume method (FVM), equations of motion for each grid cell of the generated mesh are solved to get a discretized set of conservation equations of linear algebraic. Solving this set of algebraic equations, the distribution of flow parameters within the flow field can be obtained. Quality of mesh greatly influences the overall result of CFD simulation. The local density, aspect ratio, smoothness in distribution, and skewness of all cells were checked to make sure the cells at the close proximity of the sails does not produce negative volumes or reverse local flows during calculations. In spatial discretization technique, least square cell-based gradient and second-order upwind scheme were used. For solving pressure velocity coupling, SIMPLE (Semi Implicit Methods Pressure Linked Equations) algorithm instead of PISO (Pressure Implicit Split Operator) algorithm was used since the flow was steady. RANS-based SST (Shear Stress Transport) *k*-omega turbulence model is used for this simulation. A residual of 10^{-5} is being achieved to get converged solution. In spatial discretization method Green Gauge cell-based gradient, PESTO as pressure and second-order upwind scheme were used for solution method.

8.3 Model and Mesh Description

In Figure 13a, the numerical domain for the CFD simulations in ANSYS Fluent has been shown. For these CFD simulations, the hull of the ship was not considered but all five sails were taken to consider sail–sail interaction effects. The numbering of the sail is done from forward to aft as numbers 1 to 5. The centerline of the ship is taken as the joining line of the CG of the sails. The distance from center of gravity of sail 1 to sail 5 is 5 m. The total distance between the center of gravity of first sail to fifth sail is 4.328 m and the height of sail is 1.2 m. The domain size was taken as 14 × 14 × 5 m. Keeping fluid flow in normal direction through the inlet, various combinations of sail were taken. A total number of 934 664, 1 044 910, and 992 804 cells have been used to simulate the flow field for an AWA of 120, 150, and 165°, respectively. Furthermore, three different cases were chosen for the grid indecency study to validate the results. Proximity of generated mesh distribution has been shown in Figure 13b.

Table 7 Results of stability analysis by MAXSURF software

Criteria	Minimum requirement	Light ship with sail	Before sail installation	After sail installation
Initial GM (m)	0.15	28.898	5.702	5.185
Max. GZ at 30 or greater (m)	0.200	13.206	3.309	3.155
Angle of maximum GZ (°)	25	55.5	40.9	40.9
Area (m) 0°–30°	3.151	202.957	44.715	43.374
Area (m) 0°–40°	5.157	322.811	75.573	72.306
Area (m) 30°–40°	1.719	119.854	31.794	30.856
Area *a*/area *b* (Figure 9) (%)	100	431.87	465.43	489.93

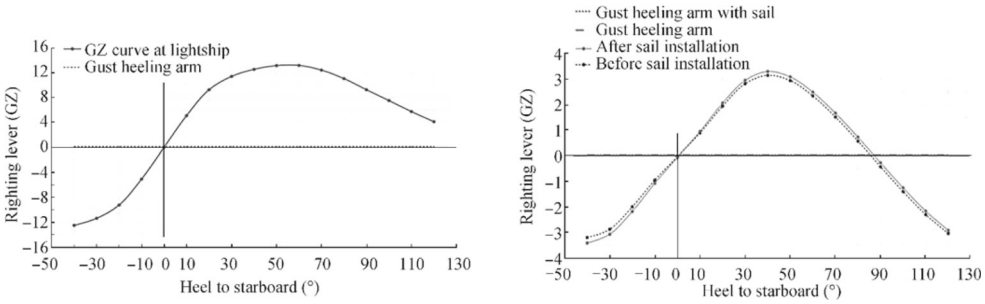

(a) Lightship condition (b) Full load condition

Figure 11 GZ curves. **a** Lightship condition. **b** Full load condition

8.4 Boundary Conditions

No slip condition was taken on sail surface. The inlet boundary was set as velocity inlet and outlet as pressure outlet. The velocity specification method was selected as magnitude, normal, and boundary. Reference frame was defined as absolute. The magnitudes of velocity were given in positive x-direction and magnitude was 2 m/s considering it as apparent wind angle for each case of apparent wind angles 120, 150, and 165°. Initial gauge pressure was set at 0 and operating pressure as 102 325 Pa. Pressure location was set up at the center of the sail centerline. The components of gravity acceleration in x- and z-directions were set as 0 and in y-direction −9.81 m/s^2 was set. The density of the air was taken as 1.225 kg/m^3.

8.5 Results from CFD Simulations: Lift and Drag Coefficient on Sails

The values of lift and drag coefficient of the sails are obtained from ANSYS Fluent and the coefficients values are plotted to observe the pattern of coefficients of sails. In each of the graphs as shown in Figure 14, along the x-axis the sail number and along y-axis the lift and drag coefficients are plotted. In Figure 14a, lift coefficients (C_L) for the AWA angle 120° has been shown and it shows that the maximum lift occurs at 30° and the minimum lift occurs at 70° sail attack angle. From Figure 14a, it is clear that there is interaction of the fluid flow on the sails of a specific sail attack angle but not significantly.

Table 8 Selected material properties

Materials	Tensile yield strength (MPa)	Tensile ultimate strength (MPa)	Young modulus (MPa)	Poison ratio	Density (kg/m^3)
Carbon fiber reinforced polymer (CFRP)	2500	3500	235 000	0.27	1850
Low alloy steel	250	460	200 000	0.30	7850

For sail attack angle 30°, minimum lift coefficient is on sail number 1 which is about 0.6779 and maximum lift coefficient is on sail number 5 which is 0.79123. In case of 70° angle of attack, the lowest lift is at sail number 1 and highest lift is at sail number 4. In Figure 14b, the drag coefficients (C_D) for AWA 120° have been shown. From the figure, it is seen that the drag coefficients for 50 and 70° angle of attack are close, but in case of 30° angle of attack, the values have a large difference from the earlier two. For AWA 150° (Figure 14c), it is seen that the lift coefficient for sail attack angle 50 and 70° are much less comparing with wind attack angle 30°. Also, there are large interaction effects on fluid flow for sail attack angle 70°. The value of drag coefficients for 50 and 70° sail attack angle is larger comparing with the drag coefficients of 70° sail attack angle (Figure 14d). Actually, comparing Figure 14c and d, it is seen that when lift greater, the drag coefficient is lesser and true for opposite case. In Figure 14e, the lift coefficients (C_L) have been shown for the case AWA 165°, and at this AWA, maximum lift occurs at 30° angle of attack and it is almost the same for all sails. However, for the 50 and 70° attack angle, the values of lift coefficients are much lesser compared to 30° sail attack angle. It is also seen that for the 70° attack angle, the lift coefficients vary most from sail to sail due to significant fluid flow interaction. That means a 70° attack angle will give maximum values of drag coefficients and most interaction will occur among the sails. The phenomenon easily can be observed from Figure 14f which represents the drag coefficient distributions for the apparent wind angle 165°. For the combination AWA 165° and sail attack angle 70°, the first sail gets the maximum drag, where in the second sail it is the lowest and then again showing a similar trend for the rest of the sails. It is apparent that at this situation, the first sail is getting the maximum wind force and due to the position of first sail and for the large wind attack angle, the first sail works as a barrier of wind for the second sail. Less interaction of wind with the second sail is the reason for which the drag force coefficient drastically reduced for that sail at this condition. So, the AWA 165, 30, and 70° sail attack angle would be desirable as higher lift produces higher forward thrust.

In Figure 15, the streamlines of the fluid flow around the sails for various combinations have been shown. Interactions

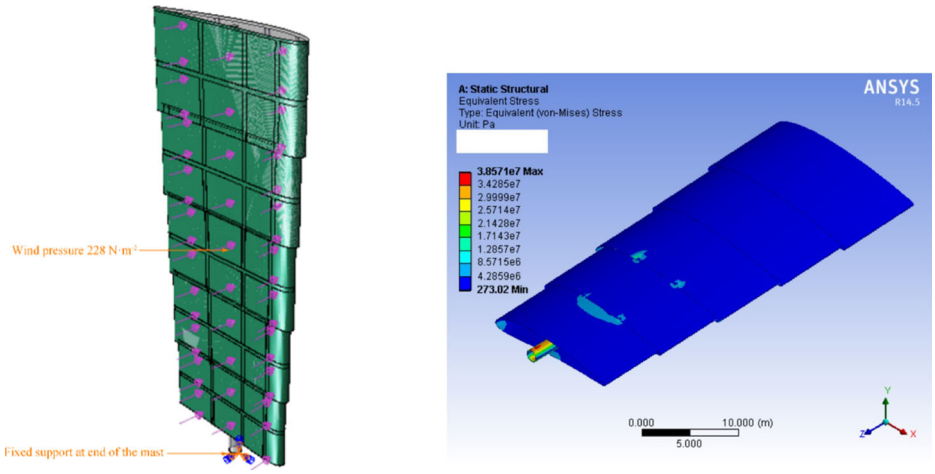

(a) Sail with uniformly distributed pressure for 15 m/s (b) Stress at sail at 15 m/s wind speed

Figure 12 Static structural analysis of sail. **a** Sail with uniformly distributed pressure for 15 m/s. **b** Stress at sail at 15 m/s wind speed

among the sails on wind flow and eddy formation at the trailing edge of the sail can be observed from the streamline. From Figure 15, it can be observed that the interaction effects among the sail is larger for lesser wind attack angle. From Figure 15a for AWA 120° with SAA 50°, it can be seen that all sails having same wind velocity and the streamlines encountered by sails are almost similar. When the AWA increased to 150° (Figure 15b), the turbulent formation behind the sails is larger than AWA 120°. For each case, the interaction among sails 3–5 is observed. Due to this interaction, there is great influence on lift and drag values as described earlier.

8.6 Thrust Distribution on Sails and Calculations of the Reduction in Forward Thrust Gained by Sails

After getting the drag and lift coefficients from CFD simulation of sails (Figure 14), the thrust coefficients for various cases of each sail were determined by using expression (5). The calculated values for each case are plotted as bar chart against sail number in Figure 16. The comparison of thrust generated by the sails for various combinations of apparent wind angle and sail attack angle states that SAA 50° for AWA 150°, SAA 70° for AWA 165°, and SAA 30° for AWA 120° produce maximum thrust. Based on these combinations, the maximum thrust coefficient values are plotted in Figure 16d. After getting the thrust coefficient value, the thrust generated by the sails was calculated using expression (3). The values collected from the experimental model test data given for JBC hull by NMRI-2015 and calculated total resistance as well as effective power and brake power of main engine have been listed in Table 4.

In Table 10, the summary of the forward thrust generated by sails for the three maximum quantities has been shown. In this table, T denotes the forward generated thrust due to sail in Newton (N) to reduce the resistance of the vessel which is calculated by using expression (3). The SAA denotes sail attack angle (°) and the percentage (%) is the amount of reduction in resistance due to forward thrust generated by sails. Percentages of deductions are obtained by comparing with the total resistance of the model ship. The thrust deduction principle is introduced to provide a measurement of the sails' ability to minimize engine-delivered thrust while maintaining the necessary forward speed. The amount of thrust deduction has been calculated as a percentage of original required thrust at service speed and defined in accordance with

$$\text{Thrust deduction} = \frac{T\ (\text{without sail}) - T\ (\text{with sails})}{T\ (\text{without sails})} \times 100\% \quad (12)$$

T (without sail) are taken at constant ship speed. Thus, percentages of thrust deduction are equivalent to a mean reduction in total resistance or effective horse power (EHP) (Fujiwara et al. 2003b). In Table 10, it is seen that about 38.25% reduction in forward thrust is possible to achieve for the model at wind speed of 1.65 m/s which accounts for about 8 m/s wind speed in case of full-scale ship for apparent wind

Table 9 Maximum deformation and stress

Wind speed (m/s)	Wind pressure (N/m^2)	Maximum deformation (m)	Maximum stress (MPa)
20	405	0.15958	69.462
15	228	0.09245	38.571

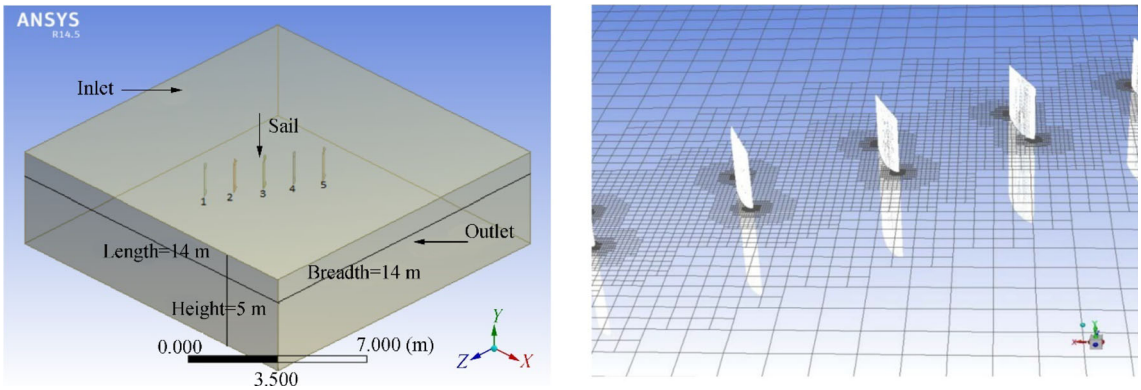

(a) Domain with Sail for AWA 180 °

(b) Mesh Distribution Around the Sails

Figure 13 Description of CFD domain and mesh. **a** Domain with sail for AWA 180°. **b** Mesh distribution around the sails

angle of 120° at sail attack angle of 50°. Again, for this case a maximum 68.64% reduction of resistance is possible to achieve at a wind speed 2.21 m/s, which will be about 12 m/s in case of full-scale ship

In case of apparent wind angle 150° with sail attack angle 70° at wind speed 1.65 m/s, about 34.52% reduction in propulsive thrust is possible and for this case a maximum of about 61.93% reduction is possible. In case of apparent wind angle 165° with sail attack angle 30° at wind speed 1.65 m/s, about 26.35% reduction in propulsive thrust is possible and for this case a maximum of about 47.26% reduction is possible.

8.7 Reduction in Engine Brake Power Calculation

The gain of a sail-assisted ship is measured in brake horse power (BHP). As a result of the additional forward thrust generated by the wing sail, less thrust is required from the propeller. The equations are given here for determining the propeller loading and corresponding engine power and fuel consumption for this off-design condition, assuming that the ship's forward speed is kept constant. The required force from the propeller of the ship with sails is determined by the longitudinal force balance (Naaijen et al. 2006):

$$X_p = R_T - X_{\text{sails}} - X_i \tag{13}$$

In above Eq. (13), X_p is the longitudnial force provided by propeller; R_T is the calm water resistance which is calculated as 28.11, and X_i is the induced longitudinal force due to drift and rudder angle which was neglected in CFD calcualtions. X_p can be expressed in terms of wake fraction and velocity of advance as

$$X_p = c_1 \left(\frac{v_a}{1-w}\right)^2 \tag{14}$$

where $c_1 = (R_T - X_{\text{sails}} - X_i)/v_m{}^2$ and v_a is velocity of advance of the ship.

Taking into account thrust deduction, the non-dimensional propeller thrust coefficient can be expressed as (Naaijen et al. 2006)

$$K_{T\text{prop}} = \frac{c_1}{(1-t)(1-w)^2 \rho D^2}.J^2 \tag{15}$$

In the above equation, velocity advance coefficient J can be solved using the propeller open water diagram by comparing the propeller's open water thrust coefficient K_T value to the above-deduced thrust coefficient $K_{T\text{prop}}$. The corresponding torque coefficient K_Q is calculated using the open water curve as shown in Figure 17. In Eq. (15), wake fraction w and thrust deduction factor t are obatined as 0.44 and 0.19, respectively, from experimental data at constant forward speed v_m 1.179 m/s. The engine brake power can be found using the expression (Fujiwara et al. 2003b, 2005)

$$P_B = \frac{\eta_{QC}}{\eta_{PC}} 2\pi\rho D^5 . K_Q . n^3 \tag{16}$$

where propeller diameter D is 0.203 m, n is propeller rotation rate in per second, P_B is brake power of engine, η_{QC} is quasi-propulsive coefficient, and η_{PC} is propulsive coefficient. Here, the ratio of propulsive coefficient is taken $\frac{\eta_{QC}}{\eta_{PC}}$ as 1.03.

The expected value of the reduced brake power as percentage is obtained using the equation

$$\text{Reduction in BP} = \frac{P_B\ (\text{without sail}) - P_B\ (\text{with sails})}{P_B(\text{without sail})} \times 100\% \tag{17}$$

P_B (without sail) is required brake power (BP) of the ship without sail at service speed and P_B (with sails) is the brake power (BP) of the ship with sails. Table 11 shows the calculated brake power and percentage in reduction of brake power

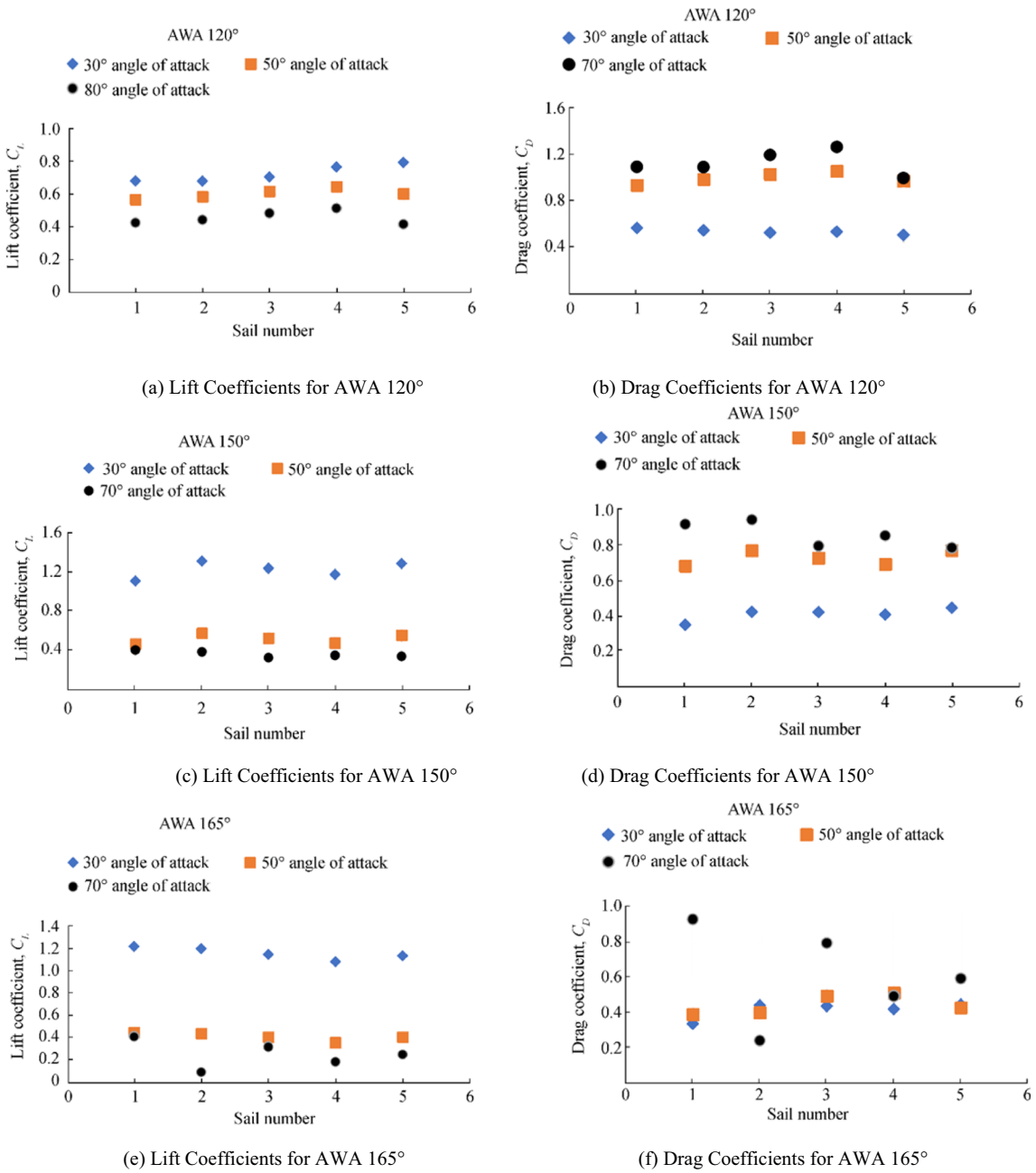

(a) Lift Coefficients for AWA 120°

(b) Drag Coefficients for AWA 120°

(c) Lift Coefficients for AWA 150°

(d) Drag Coefficients for AWA 150°

(e) Lift Coefficients for AWA 165°

(f) Drag Coefficients for AWA 165°

Figure 14 Lift and drag coefficients of sails. **a** Lift coefficients for AWA 120°. **b** Drag coefficients for AWA 120°. **c** Lift coefficients for AWA 150°. **d** Drag coefficients for AWA 150°. **e** Lift coefficients for AWA 165°. **f** Drag coefficients for AWA 165°

for a ship with five wing sails compared to a ship without any sail.

In Table 11, the brake power (BP) with sail and without sail has been calculated using above Eq. (16). In Figure 18, apparent wind speed versus brake power of engine is plotted. The horizontal red line parallel to *x*-axis shows the constant brake power of the engine at service speed. Actually, this line should not be straight because with the increase of wind speed there will be an effect on the total resistance due to wind, wave, and drift. But here, for the clear understanding of the reduction of brake power, those 7%–8% wind resistances for the higher wind speed are neglected. In Figure 18, the comparison shows the maximum reduction occurs at apparent wind angle 120° with sail attack angle 50°. For suitable wind conditions, the possible reduction in brake powers is about 9.2, 18, 27.6, and 38% at a wind speed of 0.95, 1.25, 1.65, and 1.79 m/s, respectively, for apparent wind angle 120° with sail attack angle 50°.

The economic parameters of the benefits of sail-assisted ship are expressed in terms of SFC (Fujiwara et al. 2003b). SFC is a factor of brake power of engine and depends on maximum continuous rating (MCR) of the engine. Here, SFC has been calculated by an expression based on brake

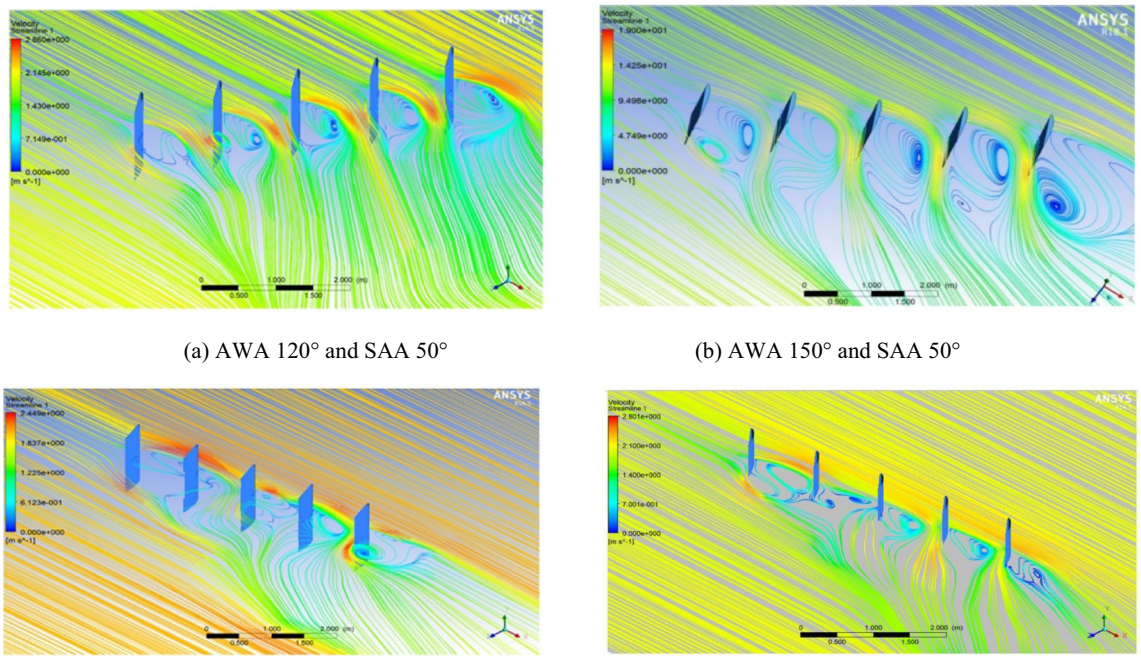

(a) AWA 120° and SAA 50°

(b) AWA 150° and SAA 50°

(c) AWA 165° and SAA 70°

(d) AWA 165 ° and SAA 30°

Figure 15 Streamlines around the sails. **a** AWA 120° and SAA 50°. **b** AWA 150° and SAA 50°. **c** AWA 165° and SAA 70°. **d** AWA 165° and SAA 30°

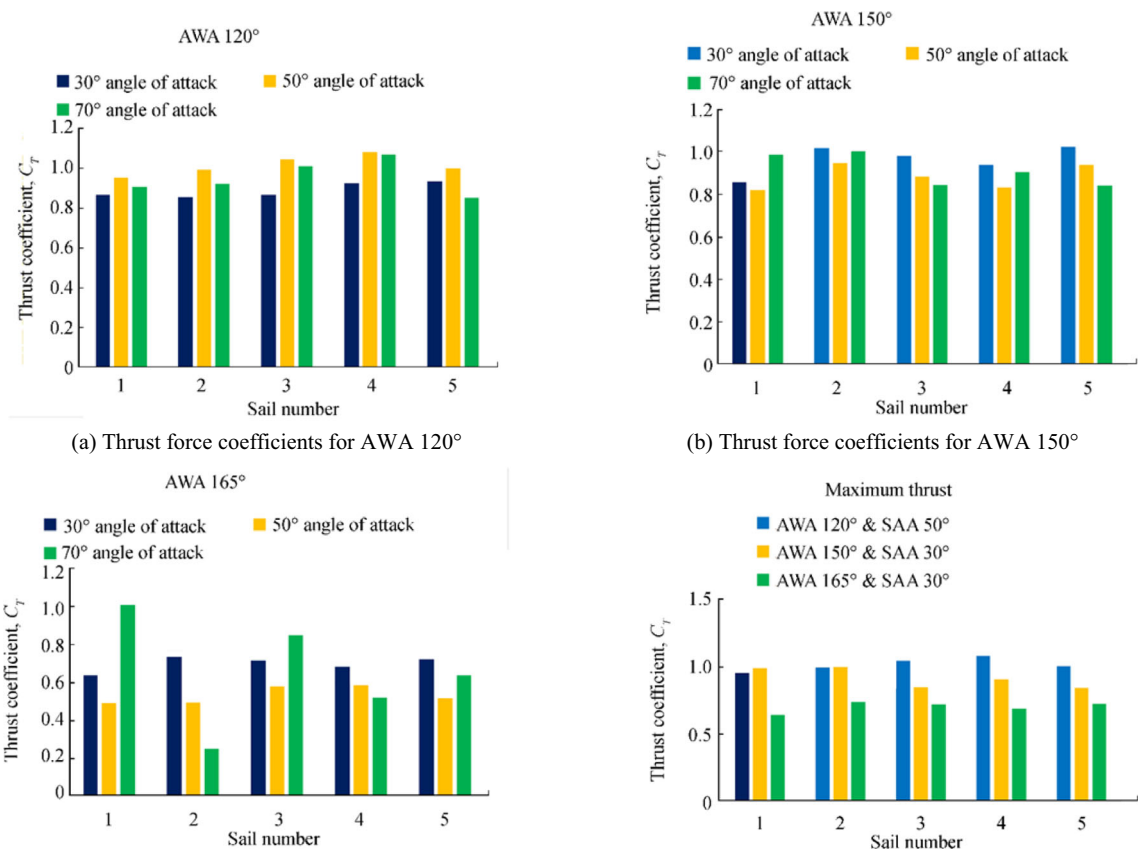

(a) Thrust force coefficients for AWA 120°

(b) Thrust force coefficients for AWA 150°

(c) Thrust force coefficients for AWA 165°

(d) Maximum thrust forces generated by sails

Figure 16 Thrust forces generated by sails**. a** Thrust force coefficients for AWA 120°. **b** Thrust force coefficients for AWA 150°. **c** Thrust force coefficients for AWA 165°. **d** Maximum thrust forces generated by sails

Table 10 Forward thrust and percentage of deduction

AWS	AWA 120°		AWA 150°		AWA 165°	
	SAA 50°		SAA 70°		SAA 30°	
	Forward thrust by sail T (N)	Deduction in R_T (%)	Forward thrust by sail T (N)	Deduction in R_T (%)	Forward thrust by sail T (N)	Deduction in R_T (%)
0.95	3.564	12.68	3.217	11.45	2.455	8.73
1.25	6.170	21.95	5.569	19.81	4.250	15.12
1.65	10.751	38.25	9.703	34.52	7.405	26.35
1.89	14.105	50.18	12.731	45.29	9.716	34.57
2.21	19.286	68.64	17.407	61.93	13.284	47.26

power of main engine proposed by Barras (2004). According to Barras (2004), fuel consumption for merchant ship with diesel machinery installation can be found as

$$\mathrm{SFC} = 0.18\, P_B \tag{18}$$

The fuel consumption of the ship without sail is found 8.68 kg/kWh. For apparent wind angle 120° with sail attack angle, the SFC values are 7.88, 7.09, 6.06, 5.23, and 3.75 kg/kWh at a wind speed of 0.95, 1.25, 1.65, 1.79, and 2.21 m/s, respectively. According to Eq. (18), the percentage of reduction in SFC will be identical as parentage of reduction brake power as shown in Table 11.

From literature review, it has been seen that the results will be influenced when interaction between sail and hull will be taken into consideration. The effects have been evaluated for particular cases of AWA 120° and discussed later in this paper.

8.8 Grid Independency Study

A grid convergence analysis is the first measure in CFD simulation result verification. Table 12 shows a comparison of the average thrust coefficient, C_T, values in five sails obtained by three different types of meshes for the grid independency analysis, and it depicts the differences in lift and drag coefficients outcome as a result of changes in the mesh used in simulations. The grid independency test was carried for the three cases of AWA 120° SAA 50°, AWA 150° SAA 70°, and AWA 165° SAA 30°. These cases were chosen for grid dependency test as the cases give maximum thrust compared to other cases of AWA and SAA. Three different grid densities from fine (S_1) to coarse (S_3) have been shown in Table 12. In meshing, the cutcell method was used to create structured mesh with a growth rate 1.2. The minimum element size of 0.08, 0.05, and 0.01 unit were taken for S_1, S_2, and S_3 grid, respectively. The maximum element size of 0.16 unit were taken for each case. In Table 10, $\varepsilon_{12}\%$ represents relative change in solution with respect to finer mesh to coarse mesh where $\varepsilon_{12}\,\%\, S_2 = |[S_2 - S_1]/S_2| \times 100$; S_2 represents finer grid. It can be seen from Table 12 that as the grids are becoming finer, a monotonous decrement of thrust coefficient value is observed. This indicates a monotonous convergence of the results as obtained from the coarse to finer mesh.

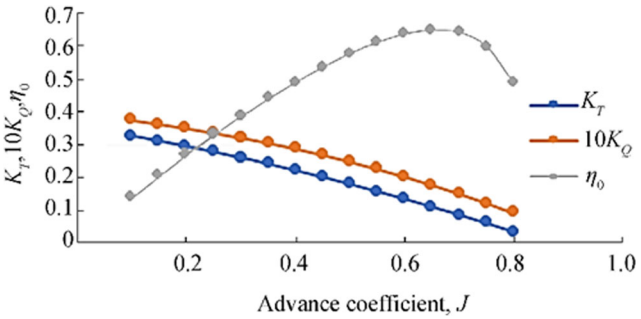

Figure 17 Propeller open water characteristics used in the calculation (NMRI 2015)

9 Sail Hull Interaction Effects

In CFD calculations, only sail–sail interaction has been considered for the prediction of the thrust generated by the sails in calm water resistance condition. To consider the effects of surge, sway, yaw, and roll on the overall propulsive efficiency of the ship with sail, the total thrust coefficient has been calculated considering the complex interactions between five sails mounted on the ship's deck and the ship itself. Due to the wind loading of the rigid wing sails mounted on a sail-assisted ship, the roll angle of freedom must be taken into consideration with surge, sway, and yaw in ship maneuvering equations. The ship maneuvering equations have been used to formulate the steady-state sailing performance as proposed by Fujiwara et al. (2005). However, in this analysis, drift force has been taken into consideration in addition to surge, sway, and yaw to investigate the effects of sail–hull interaction on the results predicted by CFD simulations. A particular case of AWA 120° at wind speed 1.89 m/s has been investigated here.

Table 11 Calculated brake powers of the ship with sails

AWS (m/s)	AWA 120°	AWA 150°	AWA 165°	AWA 120°	AWA 150°	AWA 165°
	Brake power (BP) (W)			Reduction in brake power (%)		
0.95	42.7	43.0	44.5	9.2	8.5	5.3
1.25	38.4	39.1	41.5	18.3	16.8	11.7
1.65	32.8	32.4	36.7	27.6	31.2	21.8
1.89	29.3	28.9	33.2	37.6	38.6	29.3
2.21	20.3	23.6	27.5	56.8	49.8	41.5

General form of ship motion equation in three degrees of freedom (3-DOF) can be written with respect to ship center of gravity as (Fujiwara et al. 2005)

$$m\dot{u} - mvr = X \tag{19a}$$

$$m\dot{v} - mur = Y \tag{19b}$$

$$I_{ZZ}\dot{r} = N \tag{19c}$$

The ship's mass and yaw moments of inertia with respect to the vertical z-axis and horizontal x-axis are denoted by m and I_{ZZ}, respectively, which values are presented in Tables 2, 3. The longitudinal, lateral, and yaw velocities with respect to the ship's center of gravity are denoted by u, v, and r.

Furthermore, the external forces and moments defined by the letters X, Y, and N in non-dimensional form in equation x, which include components resulting from the hull's hydrodynamic characteristics, propeller-generated thrust and torque, rudder loads, and wind forces acting on both the hull with and without sails. X, Y and N can be divided into its components due to the modular structure of the MMG model (Fujiwara et al. 2005; Sukas et al. 2019):

$$X = X_H + X_R + X_P + X_A = 0 \tag{20a}$$

$$Y = Y_H + Y_R + Y_A = 0 \tag{20b}$$

$$N = N_H + N_R + N_A = 0 \tag{20c}$$

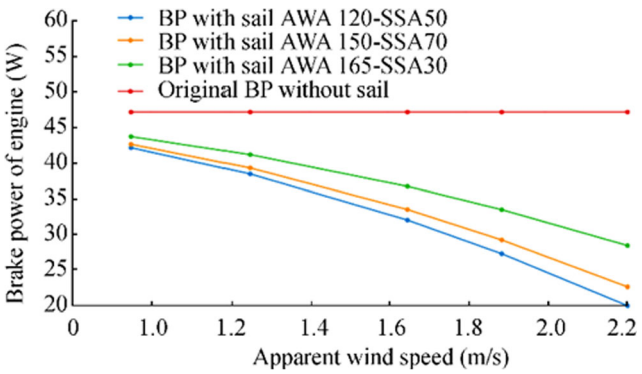

Figure 18 Brake power at different AWS for different wind and sail angle combinations

where subscript H indicates hydrodynamic forces from hull, R indicates forces from rudder, P indicates force from propeller, and A indicates force from winds. If drift and heel angle are not considered, the only hydrodynamic force from hull will be calm water resistance. While considering drift and heel angle, hydrodynamic derivatives to be taken into consideration resulting from drift and heel forces and moment in addition to calm water resistance (Fujiwara et al. 2005). The hydrodynamic derivatives were obtained by Kijima et al.'s (1990) model. Propeller open water characteristics data was used as shown in Figure 17. In case of wind-induced force and moments, the corresponding force and moment in non-dimensional form can be presented as (Fujiwara et al. 2005)

$$C_X = \frac{X_A}{\frac{1}{2}\rho_a v_a^2 A_T} \tag{21a}$$

Table 12 Grid independency study for CFD simulations of sail

Mesh	S_1 (0.4 M)	S_2 (0.65 M)	S_3 (0.93 M)	$\varepsilon_{12}\%\ S_2$	$\varepsilon_{23}\%\ S_3$
AWA 120°					
SAA 50°	C_T	C_T	C_T	7.50	4.72
	1.1427	1.063	1.0151		
Mesh	S_1				
(0.45 M)	S_2				
(0.7 M)	S_3				
(1.04 M)	$\varepsilon_{12}\%\ S_2$	$\varepsilon_{23}\%\ S_3$			
AWA 150°					
SAA 70°	C_T	C_T	C_T	6.63	3.40
	1.0104	0.9476	0.9164		
Mesh	S_1				
(0.44 M)	S_2				
(0.69 M)	S_3				
(0.99 M)	$\varepsilon_{12}\%\ S_2$	$\varepsilon_{23}\%\ S_3$			
AWA 165°					
SAA 30°	C_T	C_T	C_T	8.10	3.71
	0.7825	0.7239	0.6980		

M represents million in number of cells in each mesh

$$C_Y = \frac{Y_A}{\frac{1}{2}\rho_a v_a^2 A_L} \tag{21b}$$

$$C_N = \frac{Y_A}{\frac{1}{2}\rho_a v_a^2 A_L L} \tag{21c}$$

Initially, the wind loads on ship hull without sails were considered and next the hull with sails were combined to estimate the ship driving force in both cases. The transverse area, A_T, and lateral projected area, A_L, include total sail area when hull with sail condition was considered. The wind loads acting on the ship with sails provide estimates of wind loads with interaction of ship hull and sails.

Based on the CFD simulation results, an apparent wind angle 120° and apparent wind speed 1.89 m/s at a constant ship speed were considered in these simulations. The drift angles were taken to be 0, 5, and 10°. For each case, required forward wind thrust and total resistance were calculated as shown in Table 13. Table 13 shows the obtained forward thrust, reduction in forward thrust, required brake power, reduction in brake power, and corresponding specific fuel oil consumption for the above cases using sails. When the effects of sail–hull interaction are taken into account, there is a significant change in expected brake power and fuel savings. For AWA 120° at a wind speed 1.89 m/s, about 37.6% reduction in brake power was obtained in case of CFD simulation without taking consideration of sail–hull interaction effects (Table 11), whereas at zero-degree drift, the reduction in brake power was 26.18% for the same case of AWA and wind speed. The amount of reduction has decreased even more for drift angles 5 and 10.

10 Conclusion

The hull of Japan Bulk Carrier (JBC) was equipped with five huge hard wing sails which have vertical telescopic reefing mechanism and a self-rotating system to meet the apparent wind directions. The NACA 4412 profile was used as the section of wing sail and the numerical analysis of aerodynamic characteristics (i.e., lift and drag) of a 3D wing sail was performed by CFD simulations. By reviewing various research papers, the materials suitable for the construction of sail mast and the sail body were recommended. The structural strength of the sail was verified through static structural analysis of it under severe wind condition. The stability analysis was carried out for the sail-assisted ship by combining different stability requirements mainly focusing on the fulfillment of the weather criteria. Maximum heeling moment and the heeling moment due to wind were calculated to evaluate the weather criteria for various cases of apparent wind speed and wind direction. Intact stability analysis was done in MAXSURF software for both cases of hull before and after installation of sails and then the stability curves were compared. The results of the investigation are summarized below:

1. In case of apparent wind and sail attack angle of 90° the value of K (weather criteria) is less than 1 for wind speed 16 and 14 m/s. In case of apparent wind angle of 90° and sail attack angle of 70°, the value of K (weather criteria) is less than 1 for wind speed 16 m/s. So, these are the two cases which do not satisfy stability criteria. Otherwise, for all cases the weather criteria as well intact stability criteria are satisfied.
2. Based on aerodynamic performance and stability results, the structural analysis was carried out to check the deformation and stress in the sail. From the structural analysis of the sail, it was checked that the stress developed in the sail was lower than the yield stress of the selected material. Hence, the structural integrity of the CFRP was verified to be suitable for the construction of sail body.
3. The CFD simulations at first were carried out considering only sail–sail interaction and sail–hull interaction for drift and yaw forces were neglected. Based on 1-DOF CFD simulations, 18, 27, and 37.6% reduction of brake power are possible to achieve for model ship at wind speed of 1.25, 1.65, and 1.89 m/s, respectively, for sail apparent wind angle 120° with sail attack angle of 50°.
4. Consideration of sail–hull interaction alters the results significantly. A particular case study for AWA 120° at a wind speed 1.89 m/s shows the reduction in brake power to be about 26.18% at zero-degree drift. For higher drift angle, an average of about 20% reduction in brake power is possible. Still, it provides a significant amount of benefit in using wing sails for assisting ship propulsion.
5. Stability and structural analysis were done in full scale, but the CFD simulations to predict forward thrust

Table 13 Forward thrust, brake power, and SFC considering drift and yaw at AWA 120° for wind speed 1.89 m/s

Drift angle (°)	R_T (N)	T (forward thrust by sails) (N)	Reduction in R_T (%)	Required BP (with sail) (W)	Reduction in BP (%)	SFC (kg/kWh)
0	29.7	9.74	29.41	36.90	26.18	6.82
5	30.41	8.27	24.22	39.26	23.06	7.24
10	31.784	6.78	21.32	43.51	19.49	7.99

generated by sails were done in model scale. Ship resistance components will increase in a certain amount in full scale. Beside this, it will also have effects on the aerodynamic characteristics of sails. The scale effects must be considered before drawing precise conclusions about the sailing performance of the sail-assisted ship.

6. Therefore, in conclusion, it can be said that although it is not possible to provide a universal solution of the fuel crisis of shipping industry by using alone the wind power, it does seem to offer the greatest potential for fuel savings through the reduction in brake power and thus producing a significant amount of emission reduction. Extensive number of experimental analyses are still required to be carried out to make this technology more effective in the shipping industry.

References

Atkinson G (2012) Zero emission ship design concept with rigid sails & solar power. Aquarius MRE Systems. Available at https://www.ecomarinepower.com/en/aquarius-eco-ship [Accessed on May 02, 2020]

Barras CB (2004) Ship design and performance for Masters and Mates. 1st Ed. Elsevier Butterworth-Heinemann Press, Burlington, 132–136, Ship Trials

Bockmann E (2015) Wave propulsion of ships. PhD thesis, Norwegian University of Science and Technology, Norway, 15–16

Bordogna G, Markey DJ, Huijsmans RHM, Keuning JA, Fossati FV (2014) Wind-assisted ship propulsion: a review and development of a performance prediction program for commercial ships. Proceedings of the 11th International Conference on Hydrodynamics, ICHD 2014, Singapore, P2014–1

Carlsson L, Roggers S (2017) Wind ship sail concept could help shipowners to cut their fuel bills. Windship Technology Ltd. Available at http://www.windshiptechnology.com [Accessed on May 14, 2020]

Clearly C, Daildola JC, Reiyghling CJ (1996) Sailing ship intact stability criteria. Mar Technol 33(3):218–232. https://doi.org/10.5957/mt1.1996.33.3.218

Schmidt A (2013) Enercon E-ship 1: a wind-hybrid commercial cargo ship. Proceedings of the 4th Conference on Ship Efficiency. Hamburg, Germany, pp 23–24

Fujiwara T, Ueno M, Nimura T (1998) Estimation method of wind forces and moment acting on ship. J Soc Nav Archit Jpn 183(1998):77–90. https://doi.org/10.2534/jjasnaoe1968.1998.77

Fujiwara T, Hirata K, Ueno M, Nimura (2003a) On aerodynamic characteristics of a hybrid-sail with square soft sail. Proceedings of The Thirteenth International Offshore and Polar Engineering Conference, ISOPE2003, Honolulu, Hawaii, USA, pp 326–333

Fujiwara T, Hirata K, Ueno M., Nimura T (2003b) On development of high-performance sails for oceangoing sailing ship. Proceedings of the International Conference on Marine Simulation and Ship Manoeuvrability, MARSIM'03, Kanazawa, Japan. RC-23–1–9

Fujiwara T, Heram GE, Ueno M, Kitamura F, Minami Y (2005) Steady sailing performance of a hybrid-sail assisted bulk carrier. J Mar Sci Technol 10(3):131–146. https://doi.org/10.1007/s00773-004-0189-3

Hu Y, He J, Tang JJ, Xue S, Liu S, Wu Y (2015a) Sail structure design and stability calculation for sail-assisted ships. Marine Engineering Frontiers (MEF) 3:1–13. https://doi.org/10.14355/mef.2015.03.001

Hu Y, Tang J, Xue S, Liu S (2015b) Stability criterion and its calculation for sail-assisted ship. Int J Nav Archit Ocean Eng 7(1):1–9. https://doi.org/10.2478/IJNAOE-2015-0001

IMO (2008) Resolution MSC.267(85) (adopted on 4 December 2008) adoption of the international code on intact stability. International Maritime Organization, London, UK

IMO (2014) Third IMO GHG Study 2014 – Final Report. The International Maritime Organization (IMO), London, United Kingdom. IMO Technical Report No MEPC 67/INF.3

IWSA (2016) Wind Propulsion Innovation Awards – Archive. International Wind Ship Association, London. Available at http://wind-ship.org/en/innovation_awards/ [Accessed on February 2020]

Kijima K, Katsuno T, Nakiri Y (1990) On the maneuvering performance of a ship with parameter of loading condition. J Soc Nav Archit Jpn 168(1990):141–148. https://doi.org/10.2534/jjasnaoe1968.1990.168_141

Lloyd's Register (2015) Wind powered shipping – a review of the commercial, regulatory and technical factors affecting uptake of wind propulsion. Lloyd's Register Marine, London, UK. Available at https://wind-ship.org/wp-content/uploads/2021/02/Wind_powered_shipping_230215_LR.pdf

Lu R, Ringsberg JW (2019) Ship energy performance study of three wind-assisted ship propulsion technologies including a parametric study of the Flettner rotor technology. Ships and Offshore Structures 15(3):249–258. https://doi.org/10.1080/17445302.2019.1612544

Menter FR (1994) Two-equation eddy-viscosity turbulence models for engineering applications. AIAA J **32**(8):1598–1605. https://doi.org/10.2514/3.12149

Mofor L, Nuttal P, Newell A (2015) Renewable energy options for ship–Technology Brief. International Renewable Energy Agency (IRENA), Abu Dhabi, United Arab Emirates. Technical Report

Mohit (2017) 14 technologies to make ultimate green ship. Green shipping. Available at http://www.marineinsight.com. [Accessed on May 14, 2020]

Naaijen P, Koster V, Dallinga RP (2006) On the power savings by an auxiliary kite propulsion system. Int Shipbuild Prog 53(4):255–279

NMRI (2015) Japan Bulk Carrier hull data and conditions. Available at https://t2015.nmri.go.jp/jbc_gc.html

Nobuyuki H (2015) JBC test data in NMRI. Proceedings of the Tokyo 2015 Workshop on CFD in Ship Hydrodynamics, Tokyo, Japan, pp 23–51

Norsepower (2019) Viking Grace Rotor Sail Performance Analysis Results. Norsepower, Helsinki, Finland. Available at: https://www.norsepower.com/post/independent-tests-confirm-norsepower-rotor-sail-savings-on-viking-grace/ [Accessed on April 12, 2021]

Nuttall P, Newell A (2015) Transitioning to low carbon shipping module sustainable sea transport solutions for SIDS: Pacific Island countries case studies: United Nations Conference on Trade and Development (UNCTAD), Geneva, Switzerland. Available at http://unctadsftportal.org/wp-content/uploads/2016/08/PRINT-2a-Sea-Transport-in-the-Context-of-SIDS.pdf [Accessed on April 10, 2021]

Ouchi K, Uzawa K, Kanai A (2011) Huge hard wing sails for the propulsor of next generation sailing vessel. Second International Symposium on Marine Propulsors SMP'11, Hamburg, Germany. FA1-3

Sukas OM, Kinaci OK, Bal S (2019) Theoretical background and application of MANSIM for ship maneuvering simulations. Ocean Eng 192:106239. https://doi.org/10.1016/j.oceaneng.2019.106239

Tillig F, Ringsberg JW (2020) Design, operation and analysis of wind-assisted cargo ships. Ocean Eng 211(2020):107603. https://doi.org/10.1016/j.oceaneng.2020.107603

Van der Kolk NJ, Keuning JA, Huijsmans RHM (2019) Part 1: experimental validation of a RANS-CFD methodology for the hydrodynamics of wind-assisted ships operating at leeway angles. Ocean Eng 178(15):375–387. https://doi.org/10.1016/j.oceaneng.2018.12.041

Viola IM, Sacher M, Xu J, Wang F (2015) A numerical method for the design of ships with wind-assisted propulsion. Ocean Eng 105(2015):33–42. https://doi.org/10.1016/j.oceaneng.2015.06.009